Rapid evaluation of fatigue limit on thermographic data analysis

Jia Huang, Marie-Laetitia Pastor, Christian Garnier, Xiaojing Gong

Rapid evaluation of fatigue limit on thermographic data analysis

Jia Huang [a], Marie-Laetitia Pastor [a,*], Christian Garnier [b], Xiaojing Gong [a]

[a] Université de Toulouse, ICA (Institut Clément Ader), CNRS UMR 5312, UPS, 1, Rue Lautréamont, BP1624, 65016 Tarbes, France
[b] LGP-ENIT-INPT, Université de Toulouse, 47 Avenue d'Azereix, BP1629, 65016 Tarbes cedex, France

Keywords:
Fatigue limit
Infrared thermography
Self-heating
Data analysis

A B S T R A C T

Based on infrared thermography, the graphic methods such as Luong's method and Risitano's method are proved to be rapid and efficient for fatigue limit determination comparing to conventional methods. However, the determination procedure involves visual inspection so contains man-made uncertainties, which restricts their usage. In the present paper, we propose three new treatment methods in terms of relation curve between experimental temperature response (or dissipated energy) and the applied stress amplitude so as to determine the fatigue limit with uniqueness. Those three methods were all evaluated by applying to the experimental data from literature and the error of results were discussed and analyzed. In addition, numerical experiments were carried out to investigate the influence of loading stepped length and random error on each new treatment method.

1. Introduction

Fatigue characterization of mechanical properties is a time-consuming and costly process which is indispensable for product designing in industry. The fatigue limit, a key property of the dynamic performance of a material, is conventionally determined using the 'S-N curve' approach [1] and standard staircase method [2]. However, the traditional methods require testing a large number of specimens at different load levels [3]. It usually takes about several months and thousands of dollars to know the fatigue limit and 'S-N' curve for just one type of specimen and one type of loading. As for composites, the diversity of composites is richer than metals. So it is a very hard task to use traditional methods to optimize fiber proportion and ply scheme of composites. Therefore, various theories and rapid methods have been developed to estimate fatigue limit in a short time for both metallic materials and composites, such as X-ray method [4–7], acoustic emission method [8–11], mechanical analysis method [12–15], simulation method [16–19], and infrared thermographic method. Among that, the thermography method which is based on self-heating phenomena is most widely used in engineering applications, such as Luong's method [20–23] and Risitano's method [24–28]. Based on the curve of stabilized temperature in the specimen as a function of the applied stress amplitude ($T_{\mathrm{rstab}} = f(\sigma_a)$), Luong et al. propose to interpolate the experimental data by two lines, one for stresses below and the other for stresses above the fatigue limit, and the obtained intersection is indicated as the fatigue limit [20–23]. Whereas, Risitano's method does not take into account the temperature rising for applied stresses below fatigue limit and only utilizes one line to characterize the data of temperature rapid rising stage and the intersection of the line and x-axis is thought to be fatigue limit [24–28]. Those two graphic methods have been successfully applied to many kinds of materials and structural components, such as steels [29–31], magnesium alloy [32,33], composite materials [34–41], welded joints [42–45], riveted components [46] and components with holes [47,48]. The literature indicates that both Luong's method and Risitano's method make it possible to acquire fatigue limit within a short time and can be used for almost any stress ratio or specimen shape. Unfortunately, these procedures of graphic fatigue limit determination are controversial and questionable: How to choose the proper points to fit the lines with uniqueness? Why should we use straight lines to fit the data, not other kind of curves? The physical mechanism is not yet well understood. Thus, an optimization of graphic methods and a better understanding of the correlation between loading stress level and temperature response are required in order to better interpret experimental results. In the present paper, we develop new treatment methods of experimental data to determine the fatigue limit with uniqueness. Three improved methods were developed and applied to the experimental data found in the literature. Then the error analysis comparison of these three methods is investigated and discussed. At last, numerical experiments were conducted to evaluate the application scope of each method.

* Corresponding author.
E-mail address: marie-laetitia.pastor@iut-tarbes.fr (M.-L. Pastor).

2. Theoretical foundation and a short review of graphic methods

Fatigue behavior is irreversible process of mechanical property degradation due to cycle loading. It is concluded that fatigue damage can be defined as: (i) a chemical-physical process whereby irreversible degradation of a specific property results from the application of cyclic stress and strain, or (ii) a physical separation of the material (cracks, cavitations, etc.) [21]. These irreversible degradation and physical separation generate considerable amount of heat and this process is called intrinsic dissipation. The accumulation of dissipated energy will lead to temperature rising which can be measured by infrared thermographic camera. By combining the first and second principles of thermodynamics, the local state equation of isotropic material is deduced as [49–51]:

$$\rho C\dot{T} - \mathrm{div}(k\mathrm{grad}T) = d_i + s_{\mathrm{the}} + s_{\mathrm{ic}} + r_e \tag{1}$$

where ρ is the mass density, C the specific heat capacity, and k the heat conduction coefficient. Those three parameters are material constants and independent of the internal states. The first left-hand term of the local state equation $\rho C\dot{T}$ is the heat storage rate characterized by temperature change, and the second left-hand term $-\mathrm{div}(k\mathrm{grad}T)$ is the heat loss rate induced by conduction. The right-hand term groups characterizes the different heat sources: d_i denotes the intrinsic dissipation source; s_{the} is the thermoelastic source; s_{ic} represents the heat source induced by the coupling effect between internal variables and temperature and r_e denotes the external heat supply. For homogeneous uniaxial tests, r_e is time-independent and s_{ic} can be neglected. By assuming heat source distribution is uniform at any time within the specimen gauge part, Eq. (1) can be simplified as [49]:

$$\rho C\left(\frac{d\theta}{dt} + \frac{\theta}{\tau_{\mathrm{eq}}}\right) = s_{\mathrm{the}} + d_1 \tag{2}$$

where θ is the temperature variation at the center of the specimen gauge part; τ_{eq} characterizes all local heat losses. The temperature variation induced by s_{the}andd_1 is defined as θ_{the} and θ_{d}, respectively. For such a sinusoidal loading, θ_{the} is deduced as the sinusoidal functional form (details see Ref. [49]). Thus, the value of θ_{the} has no influence on mean temperature rising. Therefore, the stabilized shift θ_{d} can be identified as stabilized temperature rising T_{rstab}, as shown in Fig. 1. Eq. (1) also shows the dissipated heat possibly comes from micro-structural evolution. As observed by previous authors, the relationship between T_{rstab} and σ_a is non-linear. Furthermore, N. Connesson et al. [52] apply a precise measuring method and conclude the dissipated energy per cycle increases with the cumulated plastic strain while the relation between them is also non-linear. Up to now, the inherent correlation of T_{rstab} and micro-structural evolution is still not yet well understood, partly because of its complexity. In this situation, the semi-empirical graphic methods [20–28] are widely used in engineering applications, which has made many successes.

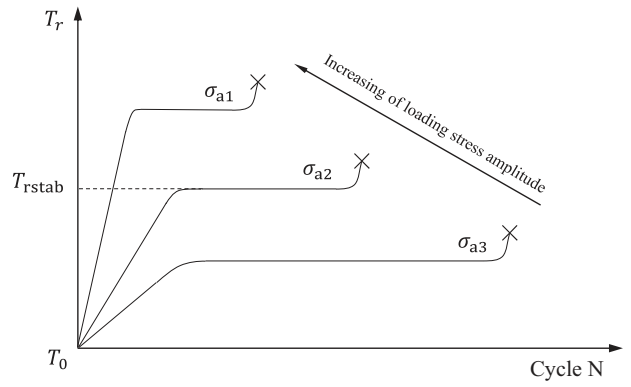

Fig. 1. Observed temperature evolution during constant amplitude fatigue tests (T_0: initial temperature).

According to previous experiments from published papers, the surface temperature of specimen's gauge section is observed to rapidly increase at the beginning of the test and then it tends to a stable value during a fatigue test. As shown in Fig. 1, with the increasing of stress amplitude, the corresponding value T_{rstab} will also increase. Since it is not necessary to run the fatigue test until specimen failures to acquire the value of stable increased temperature, the stepped loading pattern as shown in Fig. 2(a) is adopted [26]. After a certain number of load cycles, the stable value of temperature rising is recorded. Increasing the loading stress amplitude and repeating the process above, the correlation of T_{rstab} and stress amplitude σ_a, can be obtained, as illustrated in Fig. 2(b). During the whole test, the stress ratio is kept constant. Luong's method utilizes one straight line to characterize temperature response under low loading amplitude and another straight line to describe temperature rising when thermoplastic effect becomes dominant under high loading amplitude. So this method is also called two-curve method (TCM). By finding a drastic change in the rate of intrinsic dissipation, the fatigue limit can be evaluated in a very short time. Fig. 2(b) shows the determination process of Luong's method. The intersection of two straight lines is considered as the fatigue limit. As for Risitano's method, the intersection of second line and x-axis (σ_a) is fatigue limit, so it is also called one-curve method (OCM), as show in Fig. 2(b). The results of Risitano's method are relatively conservative when comparing with Luong's method [20–23].

Unfortunately, both of those two methods do not have a strict standard to divide the data into two sets of point. The common way is to find a dramatic change in the loci of T_{rstab} versus σ_a manually and separate the points into two groups. This process is usually visual and contains artificial uncertainties and different individuals may obtain distinct fatigue limit according to same experimental data. In addition, most data founded on the literature are based on temperature instead of intrinsic dissipation which is the most phenomenological approach. Therefore, in order to determine the fatigue limit with uniqueness, three new methods, based on temperature, are proposed for the treatment of experimental data.

3. Description of newly developed methodologies

3.1. Method one

If the Luong's method will be used to determine the fatigue limit, the question is how to find correctly the point that separates all experimental data into two groups. According to the hypothesis of Luong's method, the line of small slope (Line one) is used to characterize the temperature response of stress amplitude below fatigue limit and the line of large slope (Line two) is used to describe the temperature response of stress amplitude above fatigue limit, as illustrated in Fig. 2(b). Thus, we can deduce that if the points used for fitting Line one are all below fatigue limit, the slope of linear fitting is relatively similar, and if we take some points which are above fatigue limit into linear fit of Line one, the slope may change dramatically. And the same deduction is also suitable for Line two. Noticed that Luong's method is a graphic method and the relationship of slope versus the angle (θ) formed by the Line one and the x-axis (σ_a) is not linear, it is better to use angle change instead of slope change.

In order to characterize the angle change, normalized angle is used. The points on the figure of T_{rstab} versus σ_a are numbered as $P_1, P_2, P_3 \ldots P_n$ and n is the total number of points. Thus, the definition is shown as follows:

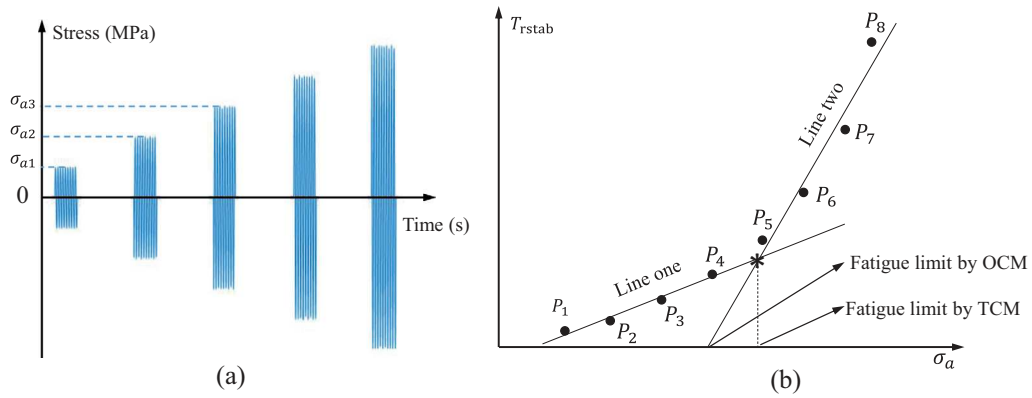

Fig. 2. (a) Schematic stepped loading process during a fatigue test for the case of $R = -1$, (b) determination of fatigue limit by graphic methods.

$$\theta_i^c = \left| \frac{\theta_{i+1} - \theta_i}{\max(\theta_{2,3,4\ldots}) - \min(\theta_{2,3,4\ldots})} \right| \quad (i \geqslant 2) \tag{3}$$

where the subscript i represents the sequence number of the points, as shown in Fig. 2(b). θ_i is the angle between x-axis (σ_a) and the line determined by point-set $\{P_{i-1},P_i\}$, as illustrated in Fig. 3. The term $\max(\theta_{2,3,4\ldots}) - \min(\theta_{2,3,4\ldots})$ is used to normalize angle change. θ_i^c is the normalized angle change between line fitted by point-set $\{P_{i-1}, P_i\}$ and point-set $\{P_i, P_{i+1}\}$. Fig. 4 gives a typical distribution of θ_i^c obtained by applying this method to the data from [40].

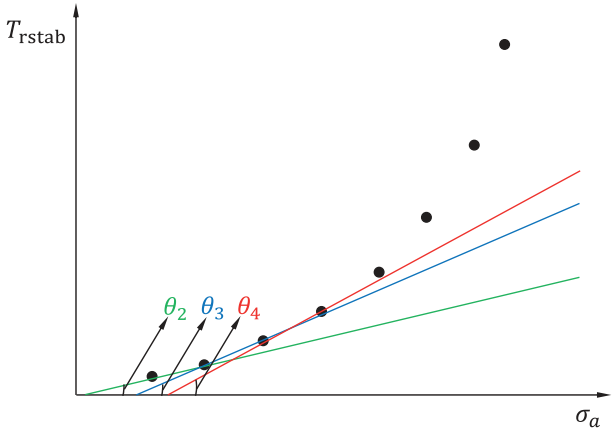

Fig. 3. Schematic definition of θ_i.

As can be seen from Fig. 4(a), if the experimental data shows a good bilinear behavior, we can easily find a peak value of θ_i^c, which means the angle changes dramatically at this point. Thus, the data can be separated into two groups by the peak node, and then Luong's method can be used to determine the fatigue limit. In addition, if the node set extends to $\{P_{i-1}, P_i, P_{i+1}\}$, the results are almost the same, as shown in Fig. 5. The results obtained by application of this method on the data from various papers are summarized in Table 1.

3.2. Method two

As it is well known, Luong et al. used two straight lines to characterize the loci of T_{rstab} versus σ_a. Thus, the gradient, $\Delta T_{rstab}/\Delta\sigma_a$, highlights a sudden change before and after fatigue limit, which may not meet the common physical facts. Therefore, we try to characterize T_{rstab} versus σ_a data using a consistent curve, so the minimum curvature radius of curve may indicate the dramatic turning point of T_{rstab}, as shown in Fig. 6.

A three parameters function was developed to characterize the curve by fitting. The expression is established as follows:

$$T_{rstab} = a \cdot \exp\left(b\sigma_a - \frac{1}{b\sigma_a}\right) + c\sigma_a \tag{4}$$

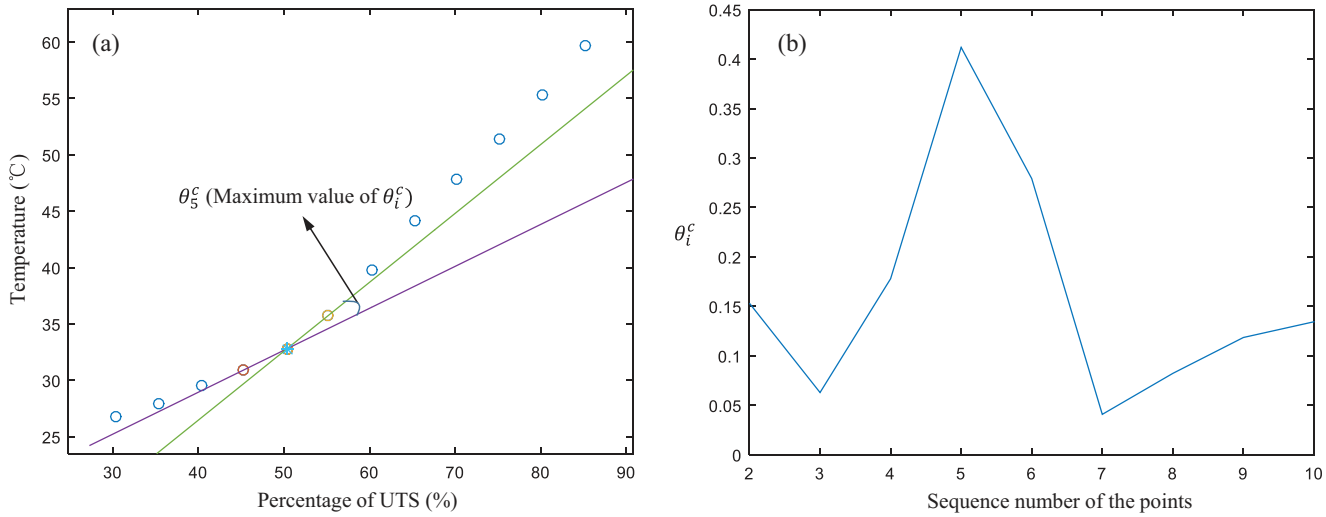

Fig. 4. A typical distribution of θ_i^c. (a) Original experimental data from [40]. (b) Loci of θ_i^c versus sequence number of point.

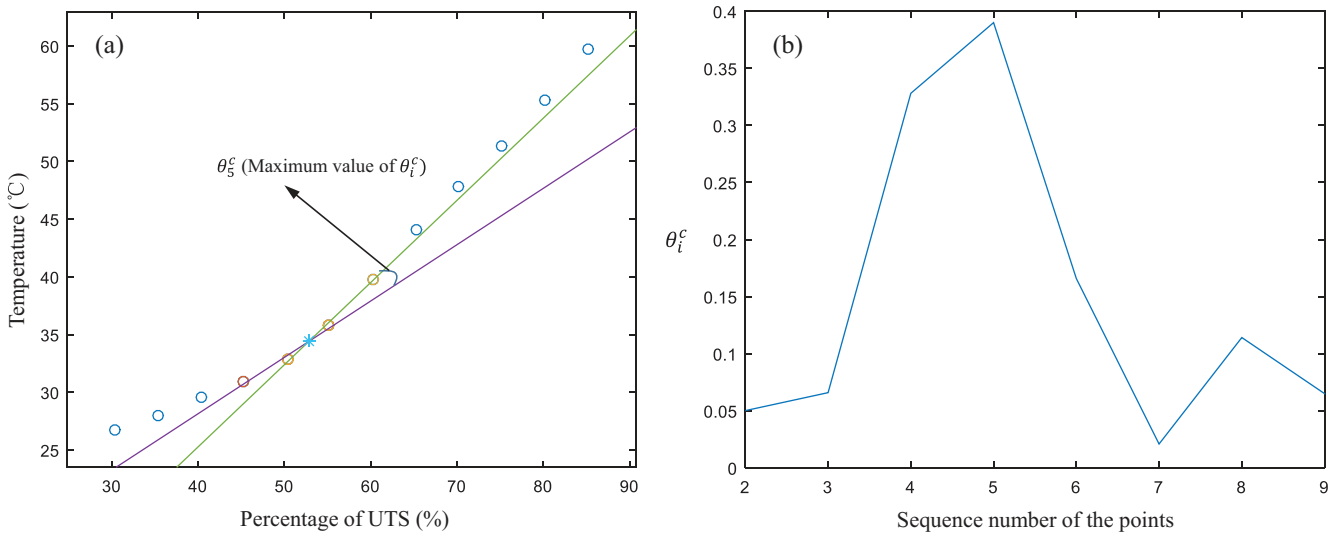

Fig. 5. The distribution of θ_i^c for the node set extending to three nodes. (a) Original experimental data from [40]. (b) Loci of θ_i^c versus sequence number of starting point.

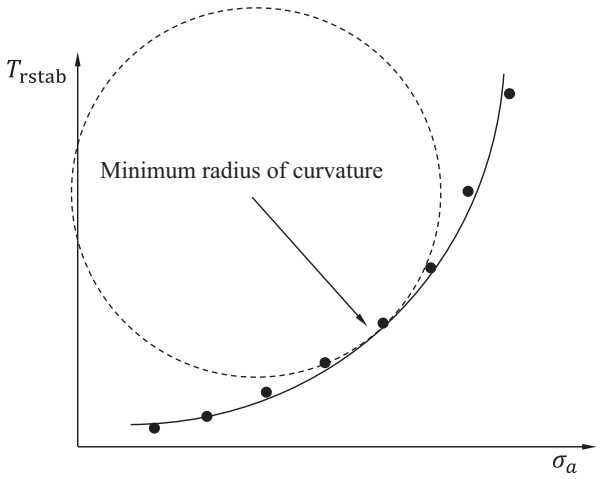

Fig. 6. Schematic definition of minimum curvature radius.

where the first term on right side is used to describe temperature response under high loading stress amplitude, and the second term on the right side is used to represent temperature rising under low loading stress amplitude. a, b, c are three parameters of interpolation to be determined. a is used to regulate the amplitude of exponential function, b is used to adjust σ_a axis range, and c is used to describe the amplitude of temperature rising in low stress cases. Thus, under the situation of low σ_a, the curve of Eq. (4) is similar to Line one, whereas, when σ_a becomes high enough, the curve of the expression is near to Line two of Luong's method. The calculation formula of curvature radius is given as follow:

$$R_\rho = \frac{1}{\kappa} = \left| \frac{(1+\dot{y})^{\frac{3}{2}}}{\ddot{y}^2} \right| \tag{5}$$

where $\dot{y} = \mathrm{dT_{rstab}}/\mathrm{d}\sigma_a$, $\ddot{y} = \mathrm{d^2T_{rstab}}/\mathrm{d}^2\sigma_a$, κ the curvature, and R_ρ curvature radius. We apply this model to experimental data from literature [34], and a typical result is shown in Fig. 7. As can be seen from Fig. 7, the fitted curve matched well with the experimental

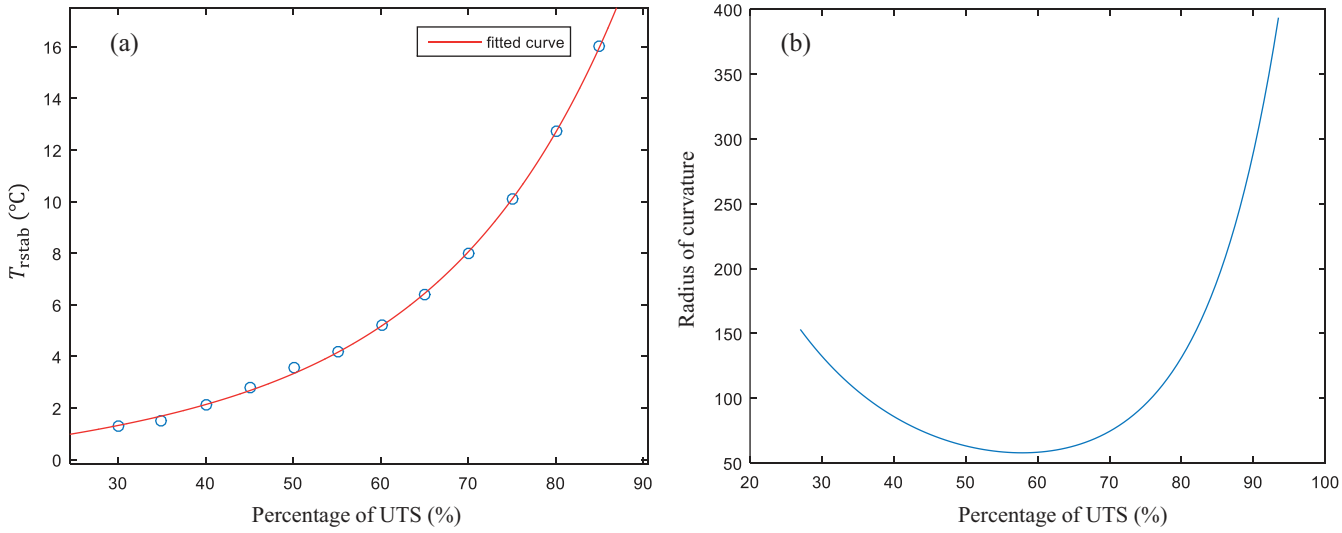

Fig. 7. A typical result of Method two. (a) The curve fitted by adopting Eq. (5) (data from [34]). (b) The loci of curvature radius versus percentage of ultimate tension stress (UTS).

data and the corresponding loci of curvature radius versus UTS can be accordingly determined. The minimum curvature radius indicates the most dramatic changing point and we naturally identified the related applied stress amplitude as the fatigue limit. The detailed results are shown in Table 1.

3.3. Method three

This method is inspired from the iterative approach proposed by Curà et al. [53]. The specific procedure of their method is held as follows:

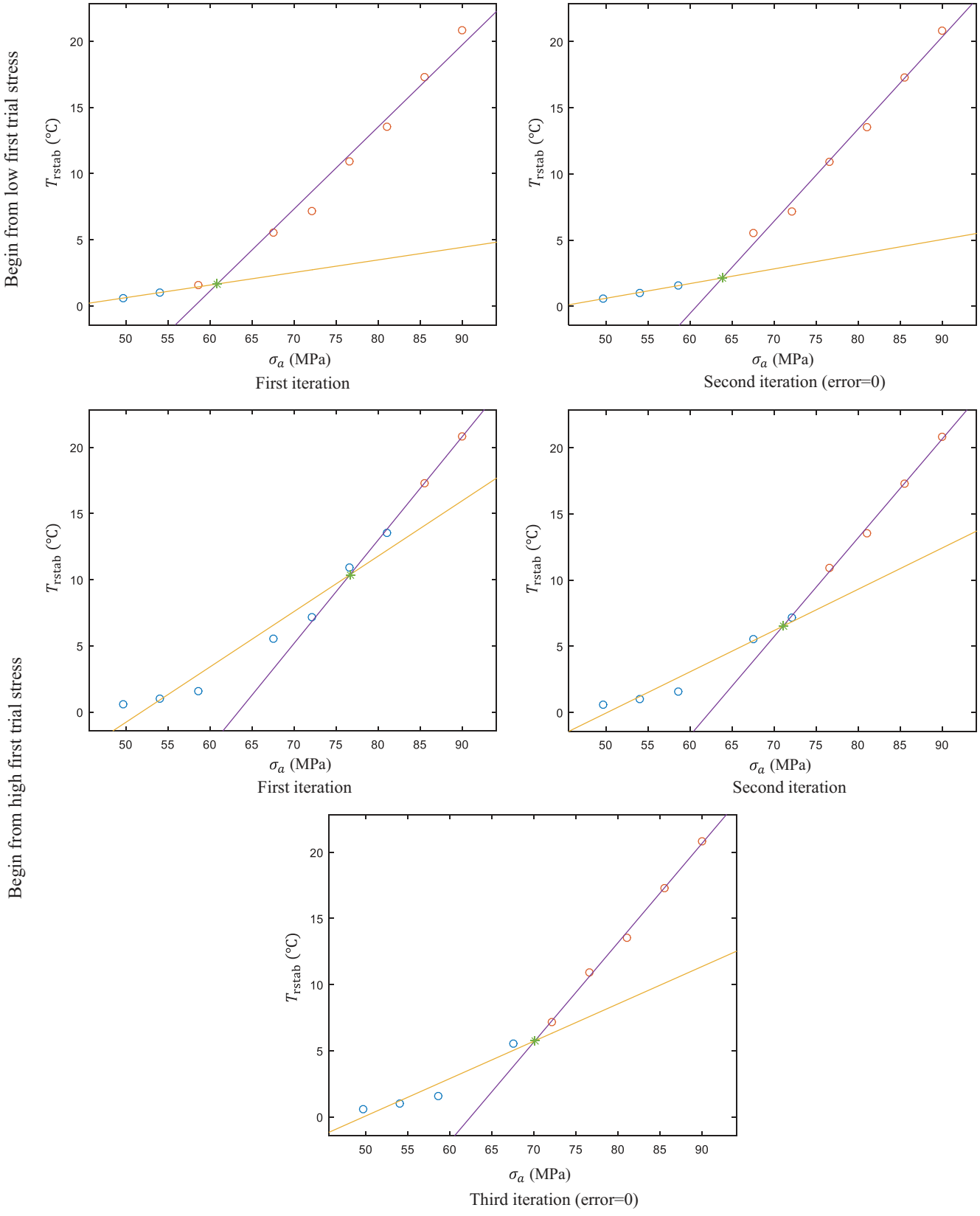

Fig. 8. The specific procedure of iteration from low and high first trial stress (data from [45]).

(1) Choose a 'first trial stress' σ_{t1}, and split the data into two groups below (Group one) and above (Group two) the value of σ_{t1}, respectively.
(2) Two different curves (straight lines) are then utilized to interpolate experimental points in those two groups and obtain the intersection as 'second trial stress', the error is defined as $\sigma_{ti} - \sigma_{t(i-1)}$.
(3) Increase (decrease) the trial stress if the error is positive (negative).
(4) Procedure stops when error is less than a prefixed value.

However, for a number of experimental results, this iterative approach may not work properly. The author does not point out step length of increasing or decreasing in step (3) and it does not tell the reader how to choose a prefixed value in the published paper. Anyway, we can set the step length as variable equaling to the error in step (4) and the prefixed error value is 0. After applying this method to the experimental data from [45], the results are shown in Fig. 8. As shown in Fig. 8 with data from [45], if the first trial stress was chosen at a low level, after twice iteration, the error is 0, whereas, for high first trial stress, after three times iteration the error is 0 as well. However, the determined fatigue limits are not the same value. So we cannot have a unique answer. In fact, for most cases, we still need to decide which one is the proper fatigue limit empirically.

Now, we try to propose a method based on statistical analysis. If two lines can well characterize the temperature rising versus stress amplitude, the goodness of fit is expected to be high. Commonly we use R^2 to evaluate the goodness of fit. The formula is expressed as:

$$R^2 = \frac{\left[\sum(X_i - \bar{X})\sum(Y_i - \bar{Y})\right]^2}{\sum(X_i - \bar{X})^2 \sum(Y_i - \bar{Y})^2} \tag{6}$$

where X_i is x-coordinate and Y_i is y-coordinate. $\bar{X}$ and $\bar{Y}$ is the mean value of X_i and Y_i, respectively. Herein, the goodness of two lines is defined as:

$$R_T^2 = (R_1^2 + R_2^2)/2 \tag{7}$$

where R_1 is the fitting goodness of Line one and R_2 is the fitting goodness of Line two. The combinations of point-sets are expressed as $\{P_1, P_2, \ldots P_k\}$ and $\{P_{k+1}, P_{k+2}, \ldots P_n\}$, where k is split point number and $2 \leqslant k \leqslant n-1$. We apply TCM to all the possible combinations and the results are shown in Fig. 9. As can be seen from the Fig. 9(b), the value of R_T^2 follows a trend of increase-highest-decrease in the whole process. The high values of R_T^2 indicate the both lines can be well fitted by the experimental data. Meanwhile, it should also be noticed that the stress amplitude σ_a corresponding to points which used to fit Line one should be lower than the determined fatigue limit while the stress amplitude of points related to Line two should be higher than fatigue limit. After excluding the combinations of point-sets do not meet the condition mentioned above, the intersection of the two lines with best goodness of fit can be considered as the fatigue limit. MATLAB© is employed here and the procedure of this method is summarized as follows:

(1) List all the possible combinations of two point-sets, such as $\{P_1, P_2, \ldots P_k\}$ and $\{P_{k+1}, P_{k+2}, \ldots P_n\}$, from original data according to split point number k;
(2) The experimental points in those point-sets will be interpolated by two different laws (linear law here) to obtain the intersection point P_i;
(3) Choose all the split combinations of two groups if $\sigma_{P_k} \leqslant \sigma_{P_i} \leqslant \sigma_{P_{k+1}}$, where σ_{P_k}, σ_{P_i} and $\sigma_{P_{k+1}}$ are the stress amplitude corresponding to points P_k, P_i and P_{k+1}, respectively (This idea is given by Curà et al. [53]);
(4) Apply goodness check (calculate R_T^2) and choose the combination with best goodness of fit, so the stress amplitude of intersection point P_i obtained from this combination is fatigue limit.

The detailed results are summarized in Table 1.

4. Results and discussion

Table 1 lists the results of fatigue limit come from the literature, based on temperature, obtained from manual graphic method and

Table 1
Summarized results of fatigue limit obtained from manual graphic method, conventional experimental method and Method 1, 2, 3.

No.	Geometry	Material	Unit	GM	TE	M1	M2	M3	$\frac{GM-TE}{TE}$	$\frac{M1-GM}{GM}$	$\frac{M1-TE}{TE}$	$\frac{M2-GM}{GM}$	$\frac{M2-TE}{TE}$	$\frac{M3-GM}{GM}$	$\frac{M3-TE}{TE}$
[45]	Flat	AZ31B Mg alloy joint	MPa	63.7	59	74.56	58.15	62.72	7.97%	*17.05%*	*26.37%*	−8.71%	−1.44%	−1.54%	6.30%
[45]	Flat	AZ31B Mg alloy joint	MPa	65.6	59.9	60.86	56.72	63.86	9.52%	−7.22%	1.60%	−13.54%	−5.31%	−2.65%	6.61%
[33]	Flat	AZ31B Mg alloy (test 1)	MPa	103.7	97.29	*Failed*	*Failed*	103.91	6.59%	Null	Null	Null	Null	0.20%	6.80%
[33]	Flat	AZ31B Mg alloy (test 2)	MPa	104.84	97.29	*Failed*	*Failed*	104.89	7.76%	Null	Null	Null	Null	0.04%	7.81%
[54]	Notched flat	SUS304 stainless steel	kN	5.8	5.7	5.81	5.70	5.74	1.75%	0.23%	1.99%	−1.78%	−0.05%	−1.05%	0.68%
[29]	Dog-bone	C55E steel (5 Hz)	MPa	420	Null	369.38	382.16	414.32	Null	−12.05%	Null	−9.01%	Null	−1.35%	Null
[29]	Dog-bone	C55E steel (10 Hz)	MPa	400	Null	394.27	366.97	407.86	Null	−1.43%	Null	−8.26%	Null	1.97%	Null
[30]	Flat	Steel DP600	MPa	293	294	294.45	266.71	286.83	−0.34%	0.50%	0.15%	−8.97%	−9.28%	−2.11%	−2.44%
[30]	Flat	Steel M800	MPa	330	333	359.82	305.84	339.18	−0.90%	9.04%	8.06%	−7.32%	−8.16%	2.78%	1.86%
[55]	Flat	Stainless steel	MPa	136	138	133.58	133.26	142.37	−1.45%	−1.78%	−3.21%	−2.02%	−3.44%	4.68%	3.17%
[31]	Flat	FV520B stainless steel	MPa	357.48	Null	357.39	327.95	357.39	Null	−0.02%	Null	−8.26%	Null	−0.02%	Null
[51]	Flat	FV520B stainless steel	MPa	346.37	339.56	344.88	330.24	355.36	2.01%	−0.43%	1.57%	−4.66%	−2.75%	2.60%	4.65%
[56]	Flat	Stainless steel	MPa	141.4	169.3	148	133.07	148	*−16.48%*	6.55%	−12.58%	−4.20%	*−21.40%*	4.67%	−12.58%
[57]	Flat	X5CrNi18-10 Steel	MPa	292.4	278.2	*Failed*	*Failed*	289.7	5.1%	Null	Null	Null	Null	−0.9%	4.10%
[58]	Dog-bone	316 L stainless steels	MPa	219	222	*Failed*	215.5	231.86	−1.35%	Null	Null	−1.60%	−2.93%	5.87%	4.44%
[59]	Flat	Aluminum 1050 H16	UTS%	75	75	73	67	72	0.00%	−2.67%	−2.67%	−10.67%	−10.67%	−2.67%	−2.67%
[59]	Flat	CMC composite	UTS%	70	Null	68	63	68	Null	−3.53%	Null	−10.00%	Null	−3.53%	Null
[37]	±45° Flat	carbon/epoxy Fabric	UTS%	50	53	68	47	52	−5.66%	*36.07%*	*28.37%*	−5.40%	−10.75%	3.52%	−2.34%
[34]	Flat	CFRP Woven	UTS%	64	63	67	58	67	1.59%	5.17%	7.69%	−9.63%	−7.46%	5.17%	7.69%
[40]	0° Flat	CFRP	UTS%	51	53	51	52	50	−3.77%	0.78%	−2.10%	2.52%	−0.40%	−1.61%	−4.42%
[41]	0° Flat	CFRP (test 1)	MPa	390	400	346.75	362.24	382.99	−2.50%	−11.09%	−13.31%	−7.12%	−9.44%	−1.80%	−4.25%
[41]	0° Flat	CFRP (test 2)	MPa	390	400	311.57	372.18	380.62	−2.50%	*−20.11%*	*−22.11%*	−4.57%	−6.95%	−2.41%	−4.85%
[36]	±45° Flat	GFRP	MPa	36	Null	37.57	33.97	37.57	Null	4.35%	Null	−5.65%	Null	4.35%	Null

UTS: Ultimate Tension Stress. Null: no available values. Failed: the method failed to generate an acceptable answer of fatigue limit. GM: Graphic Method. TE: Traditional Experiments. M1: Method one. M2: Method two. M3: Method three.

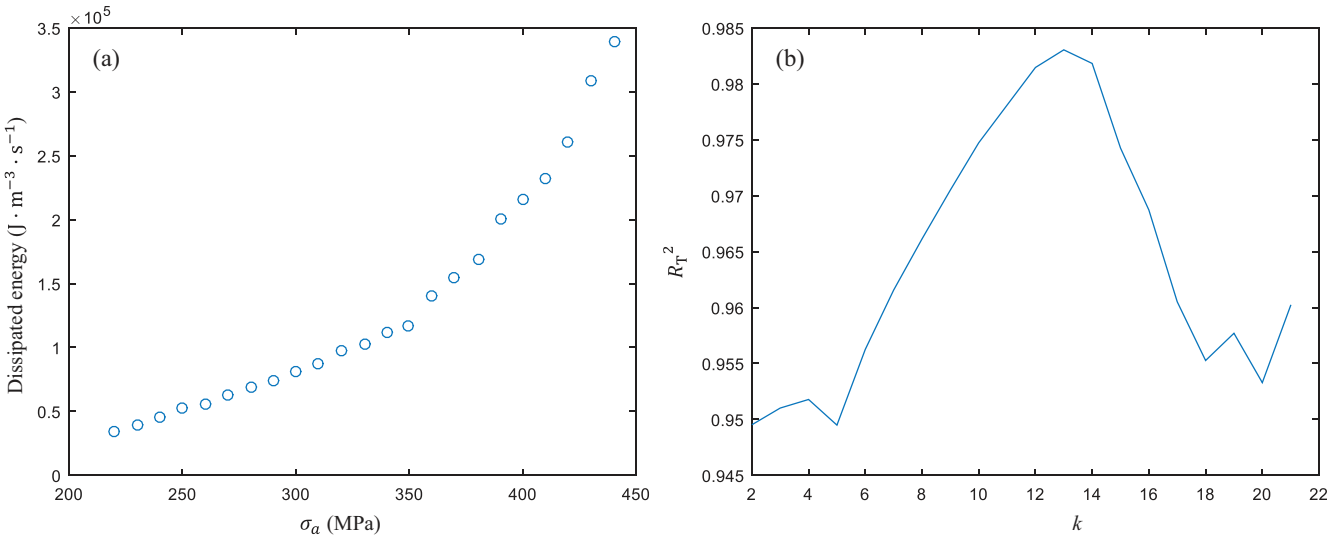

Fig. 9. Goodness of fit versus the sequence number of separated point. (a) Original experimental data from [31]. (b) Curve of R_T^2 versus split point number k.

conventional experimental method. These experimental data are also used to determine the fatigue limit by applying the three methods proposed in this paper. It is noted that except for the data in italic, the results obtained by three proposed methods in general agree well with those from the literature using the manual graphic method and conventional experimental measurement. However, there are also some drawbacks and limits in application of each method developed in present paper.

As for Method 1, the results obtained for some cases are pretty good, especially for the cases where the rising of the temperature is monotone with the applied stress amplitude, such as the data from literature [40,51,54]. But it does not work for all experimental data. If the rising of the temperature as a function of the applied stress amplitude, contains some fluctuations, the precision of the Method one can be significantly perturbed. As demonstrated in Table 1, the relative error is important when Method one is applied to the data from Refs. [37,41,45]. The method even fails to generate a proper value of fatigue limit with the data of Ref. [33] as shown in Fig. 10, because the original loci of T_{rstab} versus σ_a presents too much zigzag. In addition, it is shown that the Method one is more precise for metals than composites.

Method 2 can be applied to most of the experimental results and the error of predicted fatigue limit is acceptable on the whole of experimental data. Put it into details the predicted value of fatigue limit by Method two is always relatively less than experimental fatigue limit, especially the results of Ref. [30,37,41]. It confers to this method a conservative power. The minimum curvature radius characterizes the turning point of the curve, which indicates that dissipated energy starts to increase more and more rapidly. There is also some drawbacks. It fails to apply on the data of Ref. [33], as shown in Fig. 10. The data used to fit need to have a wide range of applied stress amplitude and enough points (usually more than 8) to ensure the stability of undetermined parameters. Moreover, this method can be applied both for metal and composite materials.

For Method 3, generally speaking, its scope of applications is widest and the error is also relatively small. For the referenced paper [37,45,54] the precision of Method 3 is even better than manual graphic method. It is suitable for almost the data from literature, and even it can work properly with the data shown in Fig. 10. Comparing the results come from the Method 3 with those from original Luong's method, the relative error is less

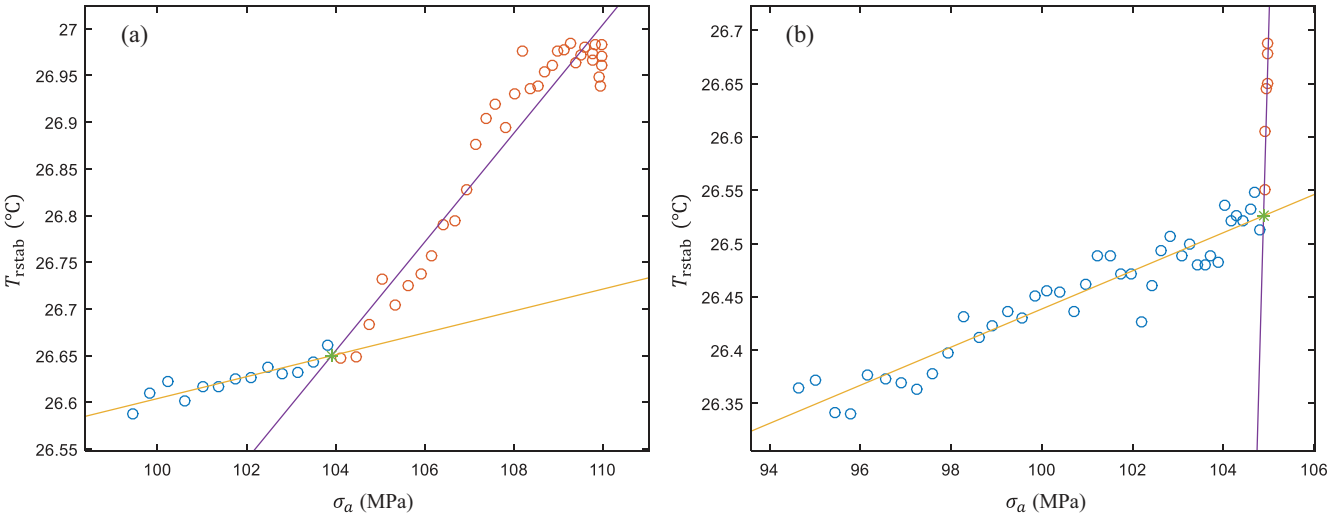

Fig. 10. Experimental data [33] of the temperature vs. stress amplitude at different stress levels and the results of fatigue limit by Method three. (a) Test one. (b) Test two.

than 6%, for all data presented in this paper (Table 1). For metallic materials, the fatigue limits determined by the Method 3 are tend to be a little higher than experimental results, whereas, for composites, there are almost equal positive and negative errors.

Since most of researchers carried out stepped loading test, as shown in Fig. 2(a), it is very important to know influence of loading stepped length as well as error disturbance on the results of those thermographic methods. In order to evaluate the influence, numerical experiments were also carried out. The experimental data in Ref. [31] were used here because the quantity of original data is up to 23 points. As shown in Fig. 9(a), the initial loading stepped length is 10 MPa. With increasing the stepped length to 20 MPa, 30 MPa, 40 MPa and 50 MPa, the results of predicted fatigue limit by each method are shown in Fig. 11. As we can observed in Fig. 11, with the increase of loading stepped length, the predicted values of fatigue limit show a trend of increasing deviation comparing to initial predicted values for all the three methods. As for method one and three, they experienced a same locus and small deviation. Even in the case of 50 MPa stepped length and we just have five available points, the predicted fatigue limit is acceptable. Whereas, Method two shows relative large deviation with the increase of loading stepped length. The decrease of data points will bring great error to the predicted results. Therefore, eight or more data points are recommended when using Method two.

During experiments, it is unavoidable to introduce some errors due to measurement or environment. Here, we introduce random error to original data in Ref. [31] and evaluate the predicted results of those three method. The maximum random error of 2%, 5%, 10% and 15% was chosen to add to original data and three parallel groups of numerical experiments were carried out to give the information of dispersion. As can be seen from Fig. 12, Method one is very sensitive to random error. When 2% and 5% of random error were introduced, the dispersion is much greater than method two and method three. If the random error is over 10%, method one failed to give correct answers. As we know, the mechanical dispersion of composites is much high than that of metals, which may lead to a poor performance of Method one on composites. However, the random error does not have large influence on Method two and Method three when the random error is no more than 10%. But in the case of 15% random error, method two showed a little better performance. The application scopes of those three methods and their points for attention are summarized in Table 2.

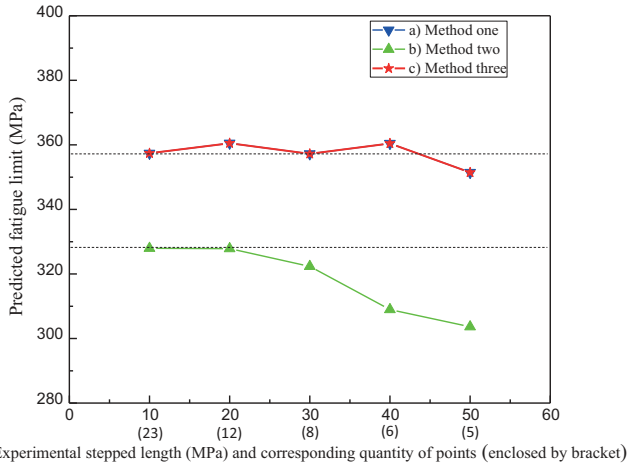

Fig. 11. The influence loading stepped length on the results of each method.

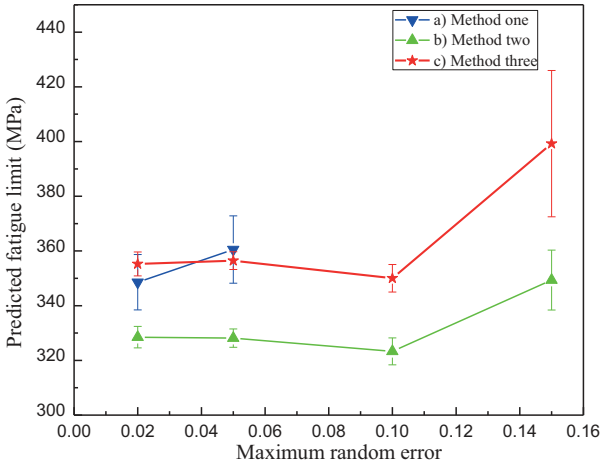

Fig. 12. The influence of random error the results of each method.

Table 2
Application scope and notices for each method.

	Application scope	Notices
Method one	Not too much zigzag and errors in original data should beless than 5%	More precise for metals than for composites
Method two	Has a wide range of σ_a and enough points on curve of original data	Predicted fatigue limit is conservative
Method three	Almost suitable for all situations	Predicted fatigue limit is not conservative

5. Conclusions

In this work, three new methods are developed in determination process of fatigue limit of material based on the measurement of temperature rise as a function of the applied stress amplitude using an infrared camera. The aim is to obtain the fatigue limit with uniqueness by using the graphic method for the rapid evaluation of fatigue limit based on thermographic data analysis. These treatment methods of experimental data are applied to a large number of experimental data found in the literature to test their efficiency and their limit. It is shown that Method one, based on the maximum angle change, can be successfully applied on the data where a monotone temperature increasing is observed as a function of the applied stress amplitude. Unfortunately, this method cannot accurately predict fatigue limits fails if the data contain measurement error and even failed when error is over 10%. For Method two, an exponential function is developed to describe the loci of T_{rstab} versus σ_a. The fatigue limit can be determined by the point having minimum curvature radius. The values of fatigue limit are usually less than that from classical experimental measurements, so it is a conservative method. Enough data points are necessary for adopting this method. Method three combines goodness of two linear laws fitting and Luong's method. This method has been applied successfully to almost all the data from literature used in this study. In terms of the thermographic data used in the present paper, the relative error between Method one and graphic method is less than 6%.

Acknowledgements

The author Jia Huang is supported by the China Scholarship Council for 3 years study at the University of Toulouse.

References

[1] Pascual FG, Meeker WQ. Estimating fatigue curves with the random fatigue-limit model. Technometrics 1999;41(4):277–89.
[2] Braam J, Van der Zwaag S. A statistical evaluation of the staircase and the arcsin $\sqrt{P}$ methods for determining the fatigue limit. J Test Eval 1998;26 (2):125–31.
[3] Feng Y, Gao C, He Y, An T, Fan C, Zhang H. Investigation on tension–tension fatigue performances and reliability fatigue life of T700/MTM46 composite laminates. Compos Struct 2016;136:64–74.
[4] Zamrik SY, Pangborn RN. Fatigue damage assessment using X-ray diffraction and life prediction methodology. Nucl Eng Des 1989;116(3):407–13.
[5] Batista AC, Nobre JP, Peixoto DF, Ferreira LA, de Castro PM, Coelho L. X-ray diffraction residual stress measurements for assessment of rolling contact fatigue behaviour of railway steels. Adv Mater Res 2014;996:782–7.
[6] Zhang H, Qu PC, Sakaguchi Y, Toda H, Kobayashi M, Uesugi K, Suzuki Y. Three-dimensional characterization of fatigue crack propagation behavior in an aluminum alloy using high resolution X-ray microtomography. Mater Sci Forum Trans Tech Publicat 2010;378–83.
[7] Bayraktar E, Antolonovich S, Bathias C. Multiscale study of fatigue behaviour of composite materials by χ-rays computed tomography. Int J Fatigue 2006;28 (10):1322–33.
[8] Mohammad M, Abdullah S, Jamaluddin N, Innayatullah O. Acoustic emission evaluation of fatigue life prediction for a carbon steel specimen using a statistical-based approach. Mater Test 2013;55(6):487–95.
[9] Kumar J, Ahmad S, Mukhopadhyay C, Jayakumar T, Kumar V. Acoustic emission studies for characterization of fatigue crack growth behavior in HSLA steel. Nondestruct Test Eval 2016;31(1):77–96.
[10] Bourchak M, Farrow IR, Bond IP, Rowland CW, Menan F. Acoustic emission energy as a fatigue damage parameter for CFRP composites. Int J Fatigue 2007;29(3):457–70.
[11] Masmoudi S, El Mahi A, Turki S. Fatigue behaviour and structural health monitoring by acoustic emission of E-glass/epoxy laminates with piezoelectric implant. Appl Acoust 2016;108:50–8.
[12] Bao K, Wang QF, Liu SL, Wei ZL. Study on local strain field intensity approach for prediction fatigue life of crankshaft based on mechanical mechanics. Adv Mater Res Trans Tech Publicat 2013;251–5.
[13] Park J, Kim S, Kim K, Park S, Lee C. A microstructural model for predicting high cycle fatigue life of steels. Int J Fatigue 2005;27(9):1115–23.
[14] Janssen RP, Govaert LE, Meijer HE. An analytical method to predict fatigue life of thermoplastics in uniaxial loading: sensitivity to wave type, frequency, and stress amplitude. Macromolecules 2008;41(7):2531–40.
[15] Akshantala NV, Talreja R. A micromechanics based model for predicting fatigue life of composite laminates. Mater Sci Eng A 2000;285(1):303–13.
[16] Lian W, Yao W. Fatigue life prediction of composite laminates by FEA simulation method. Int J Fatigue 2010;32(1):123–33.
[17] Dong H, Li Z, Wang J, Karihaloo B. A new fatigue failure theory for multidirectional fiber-reinforced composite laminates with arbitrary stacking sequence. Int J Fatigue 2016;87:294–300.
[18] Wang L, Wang B, Wei S, Hong Y, Zheng C. Prediction of long-term fatigue life of CFRP composite hydrogen storage vessel based on micromechanics of failure. Compos B Eng 2016;97:274–81.
[19] Preumont A, Piefort V. Predicting random high-cycle fatigue life with finite elements. J Vib Acoust 1994;116(2):245–8.
[20] Luong MP. Infrared thermographic scanning of fatigue in metals. Nucl Eng Des 1995;158(2):363–76.
[21] Luong MP. Fatigue limit evaluation of metals using an infrared thermographic technique. Mech Mater 1998;28(1):155–63.
[22] Luong MP. Infrared thermography of fatigue in metals. Aerosp Sens Int Soc Opt Photon 1992:222–33.
[23] Luong MP, Van KD. Metal fatigue limit evaluation using infrared thermography. In: Proceedings of workshop advanced infrared technology and applications, Capri, Italy; 1993. p. 245–53.
[24] Geraci AL, La Rosa G, Risitano A, Grech M. Determination of the fatigue limit of an austempered ductile iron using thermal infrared imagry. Digit. Photogram. Remote Sensing'95 Int. Soc. Opt. Photon. 1995:306–17.
[25] Geraci A, La Rosa G, Risitano A. On the new methodology for the determination of the fatigue limit of materials using thermal infrared techniques. Risk Minimiz. Exp. Mech. 1992:183–90.
[26] La Rosa G, Risitano A. Thermographic methodology for rapid determination of the fatigue limit of materials and mechanical components. Int J Fatigue 2000;22(1):65–73.
[27] Fargione G, Geraci A, La Rosa G, Risitano A. Rapid determination of the fatigue curve by the thermographic method. Int J Fatigue 2002;24(1):11–9.
[28] Risitano A, Risitano G. Cumulative damage evaluation of steel using infrared thermography. Theoret Appl Fract Mech 2010;54(2):82–90.
[29] Fernández-Canteli A, Castillo E, Argüelles A, Fernández P, Canales M. Checking the fatigue limit from thermographic techniques by means of a probabilistic model of the epsilon-N field. Int J Fatigue 2012;39:109–15.
[30] Munier R, Doudard C, Calloch S, Weber B. Determination of high cycle fatigue properties of a wide range of steel sheet grades from self-heating measurements. Int J Fatigue 2014;63:46–61.
[31] Guo Q, Guo X. Research on high-cycle fatigue behavior of FV520B stainless steel based on intrinsic dissipation. Mater Des 2016;90:248–55.
[32] Liu XQ, Zhang HX, Yan ZF, Wang WX, Zhou YG, Zhang QM. Fatigue life prediction of AZ31B magnesium alloy and its welding joint through infrared thermography. Theoret Appl Fract Mech 2013;67:46–52.
[33] Guo S, Zhou Y, Zhang H, Yan Z, Wang W, Sun K, et al. Thermographic analysis of the fatigue heating process for AZ31B magnesium alloy. Mater Des 2015;65:1172–80.
[34] Montesano J, Fawaz Z, Bougherara H. Use of infrared thermography to investigate the fatigue behavior of a carbon fiber reinforced polymer composite. Compos Struct 2013;97:76–83.
[35] Colombo C, Vergani L, Burman M. Static and fatigue characterisation of new basalt fibre reinforced composites. Compos Struct 2012;94 (3):1165–74.
[36] Colombo C, Libonati F, Pezzani F, Salerno A, Vergani L. Fatigue behaviour of a GFRP laminate by thermographic measurements. Procedia Eng. 2011;10 (7):3518–27.
[37] Karama M. Determination of the fatigue limit of a carbon/epoxy composite using thermographic analysis. Struct. Cont. Health Monitor. 2011;18 (7):781–9.
[38] Gornet L, Wesphal O, Burtin C, Bailleul JL, Rozycki P, Stainier L. Rapid determination of the high cycle fatigue limit curve of carbon fiber epoxy matrix composite laminates by thermography methodology: tests and finite element simulations. Procedia Eng. 2013;66:697–704.
[39] Gornet L, Westphal O, Rozycki P, Stainier L, Kemlin G. Rapid determination of the fatigue properties of carbon fiber epoxy matrix composite laminates by self heating tests. JST-AMAC-Transition statique–dynamique dans les matériaux et structures composites; 2014.
[40] Bagheri ZS, El Sawi I, Bougherara H, Zdero R. Biomechanical fatigue analysis of an advanced new carbon fiber/flax/epoxy plate for bone fracture repair using conventional fatigue tests and thermography. J Mech Behav Biomed Mater 2014;35:27–38.
[41] Peyrac C, Jollivet T, Leray N, Lefebvre F, Westphal O, Gornet L. Self-heating method for fatigue limit determination on thermoplastic composites. Procedia Eng 2015;133:129–35.
[42] Williams P, Liakat M, Khonsari M, Kabir O. A thermographic method for remaining fatigue life prediction of welded joints. Mater Des 2013;51:916–23.
[43] Crupi V, Guglielmino E, Maestro M, Marinò A. Fatigue analysis of butt welded AH36 steel joints: thermographic method and design S-N curve. Marine Struct 2009;22(3):373–86.
[44] Fan J, Guo X, Wu C, Zhao Y. Research on fatigue behavior evaluation and fatigue fracture mechanisms of cruciform welded joints. Mater Sci Eng, A 2011;528(29):8417–27.
[45] Zhang H, Wu G, Yan Z, Guo S, Chen P, Wang W. An experimental analysis of fatigue behavior of AZ31B magnesium alloy welded joint based on infrared thermography. Mater Des 2014;55:785–91.
[46] Li X, Zhang H, Wu D, Liu X, Liu J. Adopting lock-in infrared thermography technique for rapid determination of fatigue limit of aluminum alloy riveted component and affection to determined result caused by initial stress. Int J Fatigue 2012;36(1):18–23.
[47] Wang XG, Crupi V, Guo XL, Zhao YG. Quantitative thermographic methodology for fatigue assessment and stress measurement. Int J Fatigue 2010;32 (12):1970–6.
[48] Clienti C, Fargione G, La Rosa G, Risitano A, Risitano G. A first approach to the analysis of fatigue parameters by thermal variations in static tests on plastics. Eng Fract Mech 2010;77(11):2158–67.
[49] Boulanger T, Chrysochoos A, Mabru C, Galtier A. Calorimetric analysis of dissipative and thermoelastic effects associated with the fatigue behavior of steels. Int J Fatigue 2004;26(3):221–9.
[50] Chrysochoos A, Dattoma V, Wattrisse B. Deformation and dissipated energies for high cycle fatigue of 2024-T3 aluminium alloy. Theoret Appl Fract Mech 2009;52(2):117–21.
[51] Guo Q, Guo X, Fan J, Syed R, Wu C. An energy method for rapid evaluation of high-cycle fatigue parameters based on intrinsic dissipation. Int J Fatigue 2015;80:136–44.
[52] Connesson N, Maquin F, Pierron F. Dissipated energy measurements as a marker of microstructural evolution: 316L and DP600. Acta Mater 2011;59 (10):4100–15.
[53] Curà F, Curti G, Sesana R. A new iteration method for the thermographic determination of fatigue limit in steels. Int J Fatigue 2005;27(4):453–9.
[54] Ly HA, Inoue H, Irie Y. Experimental and numerical study on temperature evolution for rapid evaluation of fatigue limit. In: EPJ web of conferences, EDP sciences; 2010. p. 38007.
[55] Morabito AE, Dattoma V, Galietti U. Energy analysis of fatigue damage by thermographic technique. AeroSense 2002, Int. Soc. Opt. Photon. 2002:456–63.
[56] Kordatos EZ, Dassios KG, Aggelis DG, Matikas TE. Rapid evaluation of the fatigue limit in composites using infrared lock-in thermdography and acoustic emission. Mech Res Commun 2013;54C:14–20.
[57] Lipski Adam. Accelerated determination of the fatigue limit and the s-n curve by means of the thermographic method for X5CrNi18-10 steel". Acta Mechanica et Automatica 2016;10(1):22–7.
[58] Krapez JC, Pacou D, Gardette G. Lock-in thermography and fatigue limit of metals. Proceedings of QIRT 2000;2000:277–82.
[59] De Finis R, Palumbo D, Ancona F, Galietti U. Fatigue limit evaluation of various martensitic stainless steels with new robust thermographic data analysis. Int J Fatigue 2015;74:88–96.